Supporting Information

Interactions of the Acyl Chain with the *Saccharomyces cerevisiae* Acyl Carrier Protein

Daniel R. Perez, Marc Leibundgut, and Gerhard Wider*

Institute of Molecular Biology and Biophysics, ETH Zurich, Otto-Stern-Weg 5, 8093 Zurich, Switzerland.

* Corresponding author:

Gerhard Wider
Institute of Molecular Biology and Biophysics
Otto-Stern-Weg 5
ETH Zürich
CH-8093 Zürich, Switzerland
Telephone: +41 44 633 34 55
Email: gsw@mol.biol.ethz.ch

SUPPORTING TEXT

Protein modification measured by mass spectrometry

For the modification of apo-ScACP with different acyl-CoA species, we used an unspecific activity of the phosphopantetheinyl transferase domain from yeast (ScPPT). In ScFAS, this domain, which resides at the C-terminus of the α chain, auto-activates the multifunctional complex by transferring the phosphopantetheine group from coenzyme A (CoA) to residue Ser180 of the ACP domain in the α polypeptide (Fichtlscherer *et al.*, 2000). A crystal structure of the isolated ScPPT domain revealed the close homology to trimeric bacterial ACP synthase (ACPS) (Johansson *et al*. 2009), and we also observed that the reaction readily occurred *in vitro* using recombinantly overexpressed ScACP and ScPPT domains (Fig. S3A, top left). *In vitro* assays of this reaction further showed that ScPPT is able to attach modified versions of the substrate (like acyl-CoA of different chain lengths) to ACP, allowing to covalently attach acyl chains to ACP and obtain the same reaction intermediates that would occur upon elongation of an acyl chain in the FAS complex during fatty acid synthesis (Fig. S3A, top right).

The products of the modification reaction were analyzed by mass spectrometry (MS). The apo-form of ScACP delivers a mass of 19’660 Da corresponding to the expected molecular weight of the peptide chain without the initial methionine residue (Fig. S3B). This can be explained by the action of methionine amino-peptidase (MAP) during recombinant overexpression in *E. coli*. MAP cleaves all chains with a small side chain in the residue at the second position (in this case a glycine) (Frottin *et al*., 2006). The holo- (Fig. S3C), hexa- (data not shown), octa- (Fig. S3D), and decanoyl- (Fig. S3E) forms give an expected mass of 20’000.2 Da, 20’0128.2 Da and 20’156.1 Da, respectively. All the species show an additional peak corresponding to the replacement of a hydrogen by a potassium ion (+38.1 Da).

Thermal and chemical denaturation

Thermal denaturation. We measured the time course of the ellipticity changes in circular dichroism (CD) spectra applying a continuous temperature gradient. From measurements with different temperature gradients, we determined that the system stays at equilibrium during the measurement using 0.2 °C/min. Fig. 7A shows the temperature transition curves for apo-, holo-

and decanoyl-ScACP with denaturation midpoints at 57.1°C, 52.5°C, and 49.1°C, respectively. The results indicate that decanoyl-ScACP is less stable than holo-ScACP and apo-ScACP. However, the thermal unfolding was not reversible and aggregation occurred during the measurements.

Chemical denaturation. For a further characterization of the stability of the different ScACP forms, we used denaturation by urea, which was monitored by Circular Dichroism (CD) measurements (Fig. 7B, C, D). In addition, the chemical unfolding was analyzed by tryptophan fluorescence (Fig. 7C), which reports the unfolding of the structural domain that contains the only tryptophan in ScACP. The fluorescence and CD curves coincide (Fig. 7C), which indicates that the protein unfolds cooperatively and that a two state model is applicable. For a quantitative analysis the process has to be reversible. This is shown in Fig. 7B, where unfolding (squares) and refolding (circles) curves coincide. As shown in Fig. 7D, the protein shows an increase in stability from -4.36 ± 0.96 kcal/mol to -5.47 ± 0.59 kcal/mol when transformed from apo- to holo- form, and to -6.48 ± 1.39 kcal/mol when modified to the decanoyl-ScACP form. Although there is a tendency to stabilize the protein under acyl chain modification, the observed differences were not significant considering the error of the measurements.

Experimental setup of thermal denaturation: The thermal denaturation of ScACP in the apo- and the holo- form was monitored by CD spectroscopy using a Jasco J-710 circular dichroism spectropolarimeter (Jasco, Baltimore, MD) equipped with a Peltier thermoelectric temperature control, and a 1 mm cuvette. Equilibrium conditions were determined by changing the temperature by gradient steps of 5°C and monitor the time period required to obtain a stable CD signal. These experiments were measured with data pitch 0.2 s, bandwidth 2 nm, response 2 s, wavelength 210 nm, temperature variable, and accumulation 1. A second approach was to measure CD temperature transition curves with temperature slopes of 5°C/min, 0.5°C/min, 0.2°C/min, and 0.1°C/min and determine at which point the temperature transitions curves were stable. The rest of the measuring parameters were the same as used for the step gradient experiments.

The CD temperature denaturation transitions curves at equilibrium were measured in continuous mode, temperature slope 0.2°C/min, data pitch 0.2 s, bandwidth 2 nm, response 2 s, and wavelength 210 nm.

The transition curves were normalized using the equation:

$$y_n = \frac{(y - m_u T - y_u)}{m_f T + y_f - m_u T - y_u} \qquad [S1]$$

where y_n is the fraction of native molecules, y corresponds to the observed circular dichroism at 210 nm, y_f and y_u are the intercepts and m_f and m_u the slopes of the pre- (f) and post- (u) transition baselines, respectively, and T is the temperature.

The thermal denaturation curves were fit to equation

$$y = \frac{(y_f + m_f T) + (y_u + m_u T)\exp\left(\frac{\Delta H_m}{RT}\frac{T - T_m}{T_m}\right)}{1 + \exp\left(\frac{\Delta H_m}{RT}\frac{T - T_m}{T_m}\right)} \qquad [S2]$$

where y represents the observed circular dichroism signal at 210 nm, T_m is the transition point of the thermal unfolding curve and ΔH_m is the enthalpy change for unfolding at T_m, for a two state and reversible thermal unfolding (Santoro and Bolen, 1988).

Experimental setup of chemical denaturation. The chemical denaturation at equilibrium was measured by CD spectroscopy at 220 nm. The protein samples contained 5 μM ScACP in 20 mM potassium phosphate at pH 6.5 and were titrated with urea from 0.1 M to 8 M. For each measured point the urea concentration was determined by measuring the refractive index and using the following relation (Warren & Gordon 1966):

$$Urea[\mathrm{M}] = 117.66(\Delta\eta) + 29.753(\Delta\eta)^2 + 185.56(\Delta\eta)^3 \qquad [S3]$$

where $\Delta\eta$ corresponds to the difference in the refractive index between the denaturant solution and the reference buffer at the sodium D line. The experimental data were normalized in the same way as described for the thermal denaturation using equation [S1].

The chemical denaturation measurements were repeated three times, and the three datasets were fitted independently to the following equation:

$$y = \frac{(y_f + m_f[D]) + (y_u + m_u[D])\exp\left(\frac{[D]-[D]_{1/2}}{RT}\right)}{1+\exp\left(\frac{[D]-[D]_{1/2}}{RT}\right)} \qquad [S4]$$

where y correspond to the observed ellipticity at 220 nm, y_f and y_u are the intercepts and m_f and m_u are the slopes of the pre- and post-transition baselines, respectively, $[D]_{1/2}$ is the urea concentration at the transition point of the curve, and m_f the cooperativity, a measure of the dependence of ΔG on urea concentration (Pace *et al.*, 1998). For the graphical representation of the results, the intercepts and slopes obtained with the previous procedure were used to normalize the data with equation [S1].

Using the normalized transition curve and assuming a two state model, the values of the equilibrium constant were calculated from the folded fraction α using the relation:

$$K_{eq} = \frac{[\mathrm{N}]}{[\mathrm{U}]} = \frac{1-\alpha}{\alpha} \qquad [S5]$$

with the value of α being significantly different from 0 or 1. This provides the free energy of folding ΔG for each point of the denaturing transition by:

$$\Delta G = -RT \ln(K) \qquad [S6]$$

Finally, the free energy of the folded relative to the unfolded state in water ΔG_{H2O} is obtained by extrapolating ΔG to 0 M urea using (Creighton, 1992):

$$\Delta G = \Delta G_{H2O} - m\,[D] \qquad [S7]$$

where *m* is the cooperativity value obtained by equation S4.

SUPPORTING FIGURES

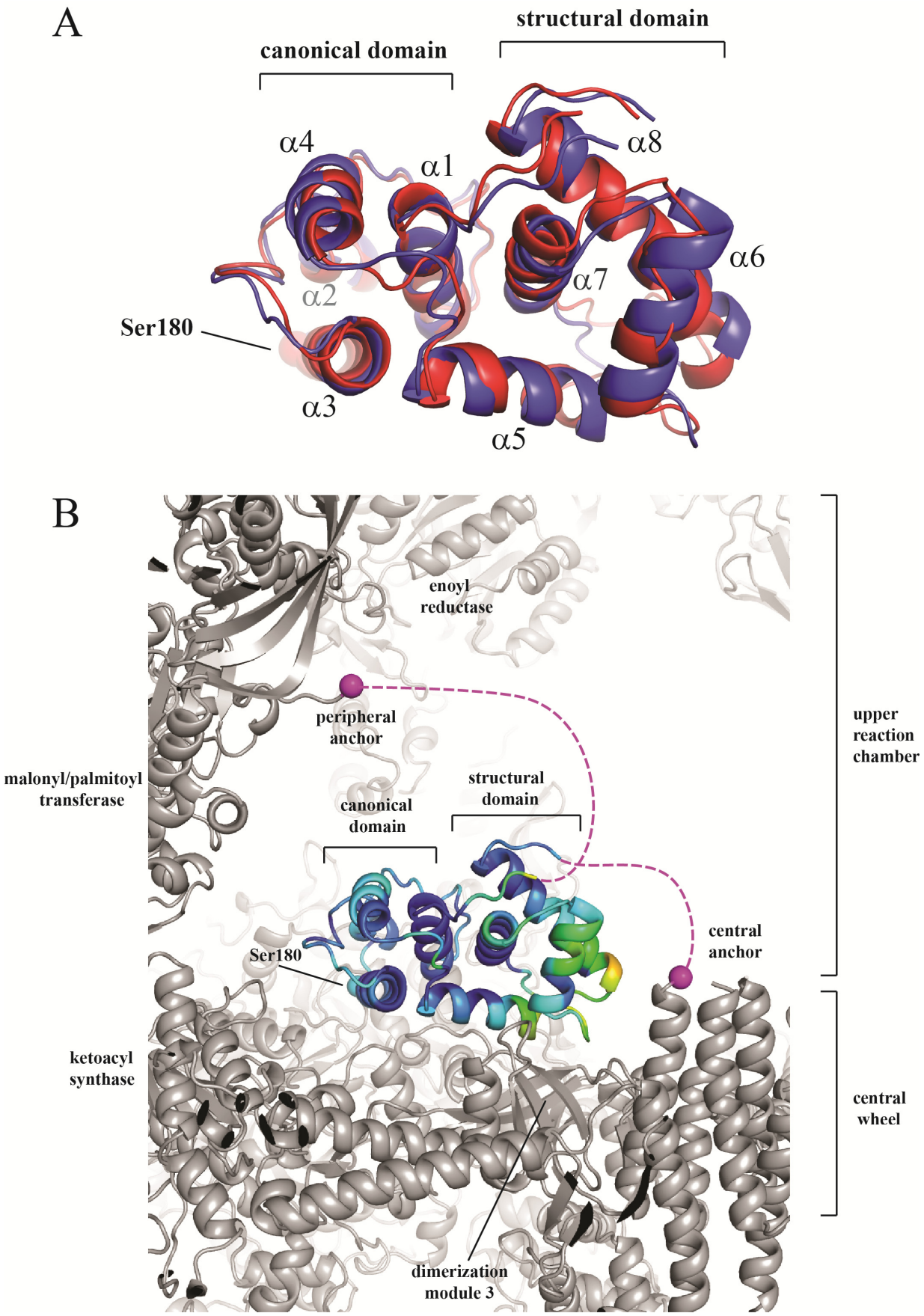


Fig. S1

Comparison of the structures of the ScACP domain determined in solution and the ScACP domain in the context of the FAS complex. (A) The superposition of the crystal structure (blue) with the mean structure of the bundle of 20 NMR conformers (red) reveals a very similar overall fold (the r.m.s.d. is 2.06Å for all C_α atoms), with the canonical and structural ScACP subdomains arranged in the same orientation relative to each other. The superposition was performed using LSQKAB (Kabsch, 1976). (B) Structural differences between the NMR structure and the ScACP stalled in the FAS complex. The deviations of the C_α atoms are plotted onto ScACP in the crystal structure (PDB ID 2UV8) as a color gradient reaching from low (blue) to high (red) r.m.s.d. Largest deviations are observed in the structural subdomain of ScACP, which is in contact with the central wheel. The flexible linkers, which were not viusualized in the crystal structure, are shown schematically as dashed magenta lines.

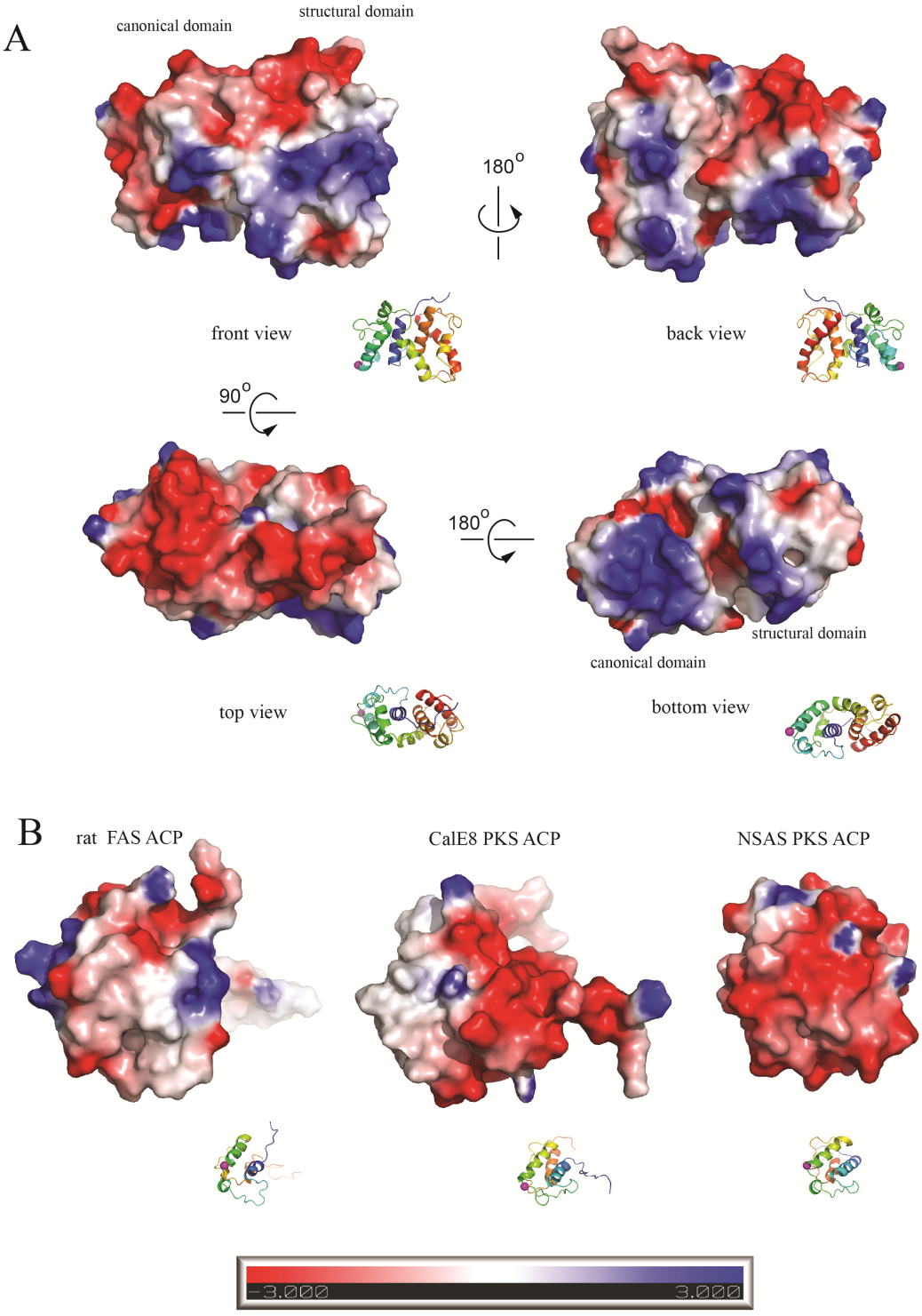


Fig. S2

Surface potentials of ACP domains from different type I FASs and multifunctional PKSs. (A) Surface potential of one of the NMR conformers of ScACP displayed from various sides (for better orientation, the structures are shown as cartoon in the insets). The bottom view reveals a

large, positively charged patch encompassing both the structural and the canonical ScACP subdomain, which is in contact with the negatively charged central wheel in the FAS complex (Leibundgut *et al*., 2007), while the top of ScACP carries a strong negative charge. (B) Bottom views of the surface potentials of other type-I ACPs shown for comparison: PDB IDs 2PNG (rat FAS ACP), 2LF9 (*Micromonospora echinospora* CalE8 PKS ACP, 2KR5 (*Aspergillus parasiticus* NSAS PKS ACP). The charge distribution differs considerably between the ACPs of the multienzymes, which may be an adaptation to their specific functions or different overall architectures. The surface potentials were calculated using DelPhi (Rocchia *et al*., 2002) and visualized using PyMOL (Schrödinger, 2010).

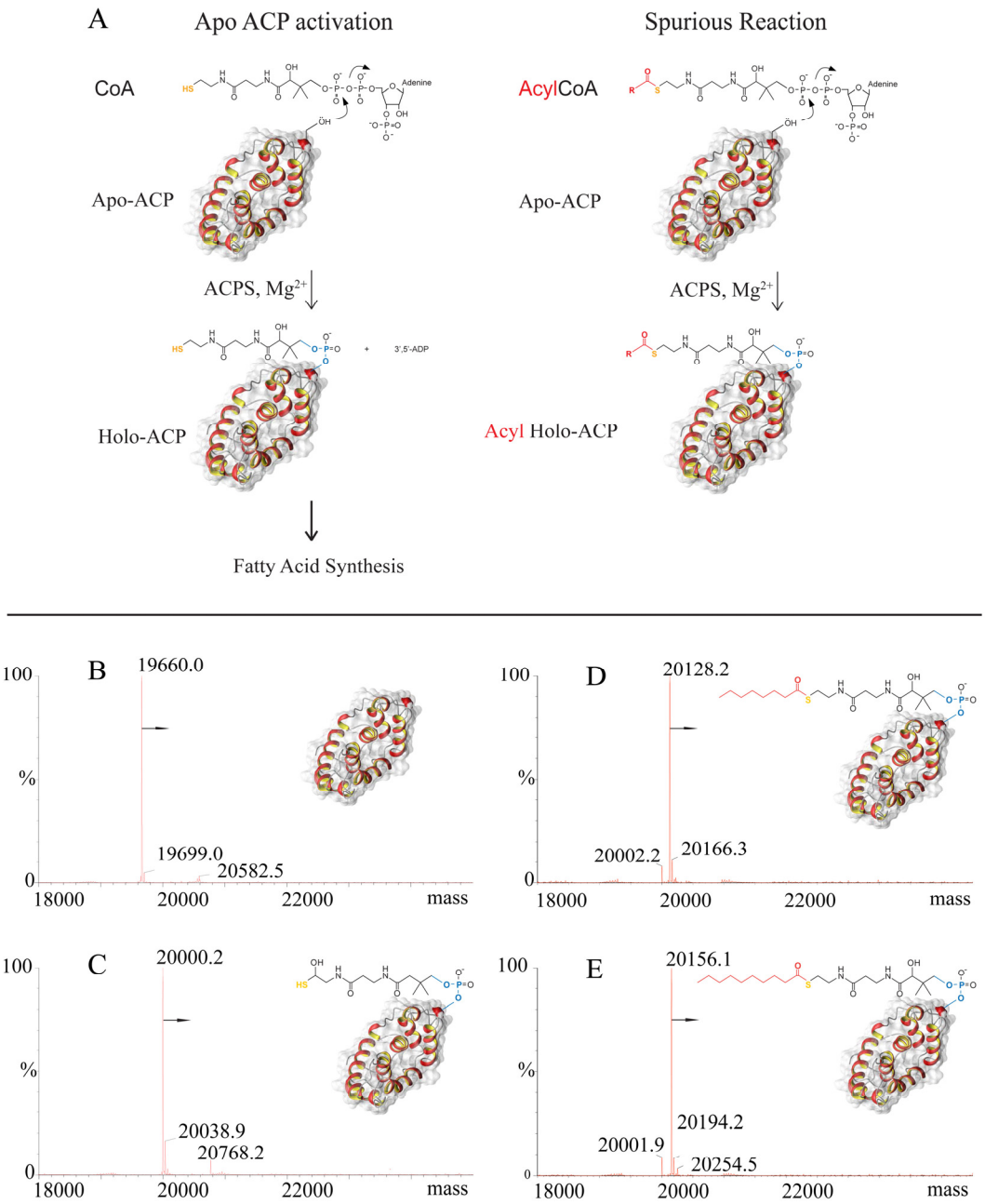


Fig. S3

Apo- to holo- and acyl-ScACP modification controlled by mass spectrometry. (A) Natural reaction catalyzed by yeast phosphopantetheine transferase (ScPPT) *in vivo* (left), spurious unspecific reaction obtained *in vitro* (right). Lower panel: MS spectra for (B) the purified apo-ScACP, and (C) the transformed holo-ScACP, (D) the transformed octanoyl-, and (E) the transformed decanoyl-ScACP; the determined masses are indicated and correspond to the ones expected within 0.1 mass units. The NMR mean structure was used for the representation of the structure of ScACP, which was drawn using MOLMOL (Koradi *et al.*, 1996).

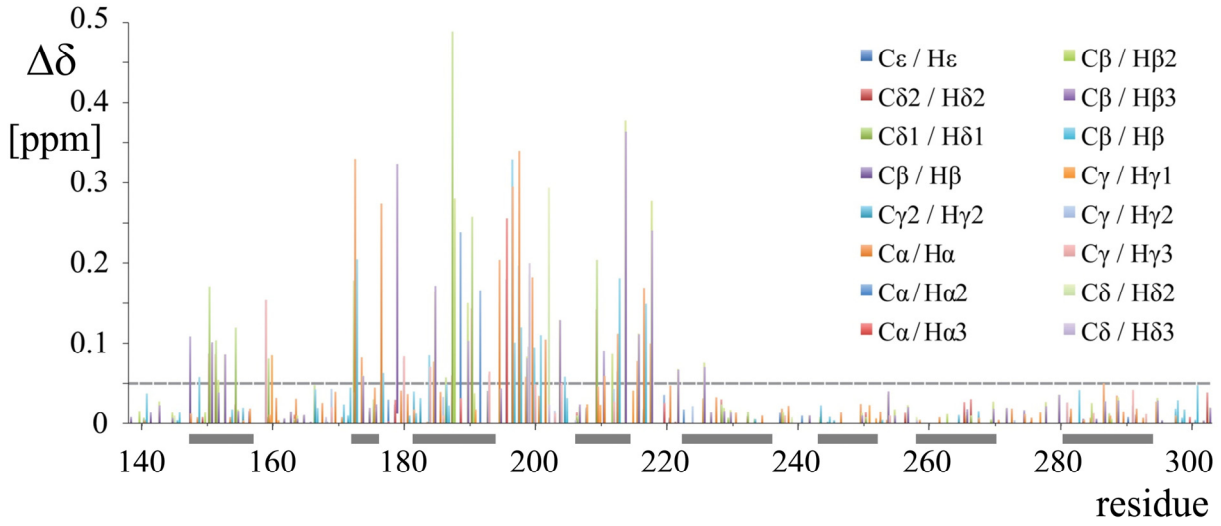


Fig. S4

Plot of the chemical shift perturbations, Δδ, between ScACP holo- and decanoyl-forms versus the amino acid sequence. The combined chemical shift perturbations of ^{1}H, $\Delta\delta(H_C)$, and ^{13}C, $\Delta\delta(C)$, calculated with the formula $[(\Delta\delta(H_C)^2 + (\Delta\delta(C)/2)^2]^{1/2}$ (Schumann et al., 2007) are shown; an arbitrary threshold of 0.05 ppm was used to define changes considered significant; different colors were used for different types of CH moieties as indicated in the figure. The horizontal gray bars represent the positions of the 8 α helices in ScACP.

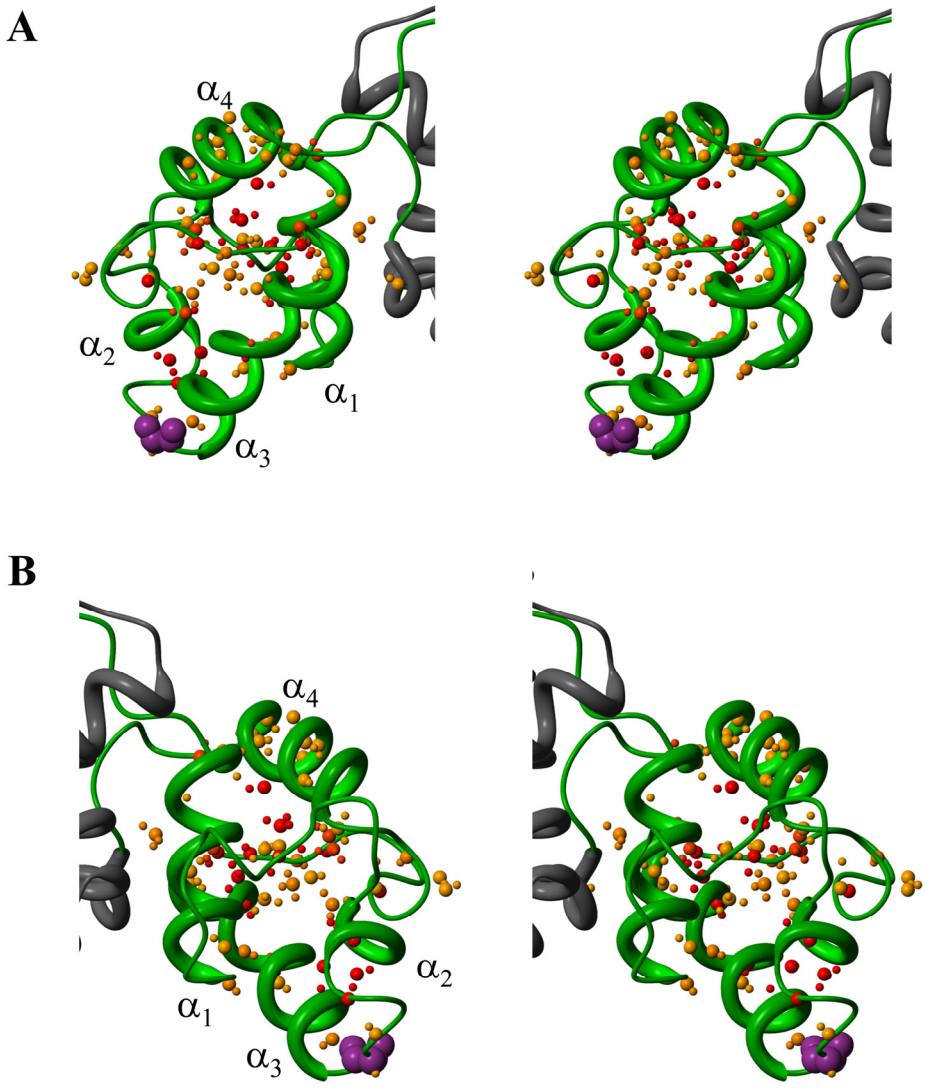


Fig. S5

Combined chemical shift perturbations, Δδ, of NH- / CH-moieties between [^{1}H,^{15}N]- / [^{1}H,^{13}C]- HSQC spectra of ScACP holo- and decanoyl-forms mapped on a stereo view of the NMR structure. The canonical domain is colored in green and the structural domain in gray (shown only partially). All atoms with significant Δδ values (see Fig. 3 and S4) are shown as small spheres using the following color code; orange: $0.05 \leq \Delta\delta \leq 0.2$ ppm and red: $\Delta\delta > 0.2$; heavy atoms N and C are shown with larger spheres than hydrogen atoms. Magenta spheres represent Ser180, where the phosphopantetheine group (not shown) is attached. The stereo view in panel A shows the same orientation of the molecule as in Fig. 1; panel B presents the back side after a 180° rotation around a vertical axis in the paper plane.

SUPPORTING TABLES

Table S1

Input for structure calculation and characterization of the energy-minimized NMR structures of ScACP.

Quantity	Value[a]
NOE upper distance limits	
total	3713
intraresidual	876
sequential (|i-j|=1)	995
medium range (1<|i-j|<5)	931
long range (|i-j|>=5)	911
Hydrogen bonds	0
Torsion angles	0
Residual target function, ($Å^2$)	1.12 ± 0.17
Residual NOE violations	
number (≥ 0.2Å, ≤ 0.3Å)	2.6 ± 1.3
maximum, (Å)	0.28 ± 0.05
AMBER energies, (kcal/mol)	
total	-3941 ± 22.7
van der Waals	-1159 ± 13.6
electrostatic	-12771 ± 251
R.m.s.d. to the mean coordinates for residues 140-302 (Å)	
N, C^{α}, C^{γ} (backbone)	0.53 ± 0.07
all heavy atoms	0.82 ± 0.07
Ramachandran plot statistics[b], (%)	
most favored regions	88.5 ± 1.4
additional allowed regions	11.1 ±1.6
generously allowed regions	0.5 ± 0.4
disallowed regions	0.0 ± 0.0

[a] Except for NOE distance limits, hydrogen bonds and torsion angles, the average value for the 20 energy-minimized conformers and the standard deviation among them are given for residues 140–302.

[b] As determined by PROCHECK (Laskowski *et al*, 1996).

Table S2:

Comparison of the yeast ACP NMR structure (PDB ID 2ML8) with selected type I and type II ACPs from other organisms. For the structure-based alignments, yeast ACP residues 140-198 of the average from the deposited ensemble of 20 structures were used.

PDB ID (type of structure)	Organism (origin of ACP)	C_α r.m.s.d.[#] (Å)	Identity [#] (%)
Type I ACP			
2UV8 (X-ray)	Yeast (FAS)		
ACP domain		2.06	100
canonical subdomain		1.16	100
structural subdomain		2.40	100
2L9F (NMR)	*Micromonospora echinospora* (CalE8 PKS)	2.66	17
2PNG (NMR)	Rat (FAS I)	3.02	18
2KR5 (NMR)	*Aspergillus parasiticus* (NSAS PKS)	2.76	10
Type II ACP			
1L0H (X-ray)	*E. coli* (FAS II)	2.10	12
2FVE (NMR)	Spinach (FAS II)	2.70	18
2K0Y (NMR)	*Streptomyces coelicolor* (Actinorhodin PKS)	2.89	14

[#] determined using the secondary structure based PDBeFOLD server at EBI (http://www.ebi.ac.uk/msd-srv/ssm (Krissinel *et al.*, 2004)) except for yeast ACP, for which all residues from 140-302 (entire domain), 140-198 (canonical subdomain) and 199-302 (structural subdomain) were superimposed using LSQKAB (Kabsch, 1976).

SUPPORTING REFERENCES

Creighton TE. (1992) Proteins, structures and molecular properties. 2nd Ed. W.H. Freeman, WH & Company, New York, USA.

Fichtlscherer F, Wellein C, Mittag M, Schweizer E. (2000) A novel function of yeast fatty acid synthase. Subunit alpha is capable of self-pantetheinylation. Eur J Biochem. 267: 2666–2671.

Frottin F, Martinez A, Peynot P, Mitra S, Holz RC, Giglione C, Meinnel T. (2006) The proteomics of N-terminal methionine cleavage. Mol. Cell. Prot. 5: 2336–2349.

Johansson P, Mulinacci B, Koestler C, Vollrath R, Oesterhelt D, Grininger M. (2009) Multimeric options for the auto-activation of the Saccharomyces cerevisiae FAS type I megasynthase. Structure 17: 1063–1074.

Kabsch W. (1976) Solution for best rotation to relate 2 sets of vectors. Acta. Cryst. A32, 922–923.

Krissinel K, Henrick K. (2004) Secondary-structure matching (SSM), a new tool for fast protein structure alignment in three dimensions. Acta Cryst. D60, 2256–2268)

Koradi R; Billeter M; Wüthrich K. (1996) MOLMOL: A program for display and analysis of macromolecular structures. J Mol Graphics 14: 51–55.

Leibundgut, M., Jenni, S., Frick, C., Ban, N. (2007). Structural basis for substrate delivery by acyl carrier protein in the yeast fatty acid synthase. Science 316, 288-290.

Laskowski RA, Rullmann JAC, MacArthur MW, Kaptein R, Thornton JM. (1996) AQUA and PROCHECK-NMR: Programs for checking the quality of protein structures solved by NMR. J. Biomol. NMR 8: 477–486.

Pace CN, Hebert EJ, Shaw KL, Schell D, Both V, Krajcikova D, Sevcik J, Wilson KS, Dauter Z, Hartley RW, Grimsley, GR. (1998) Conformational Stability and Thermodynamics of Folding of Ribonucleases Sa, Sa2 and Sa3. J Mol Biol 279: 271–286.

Rocchia W, Sridharan S, Nicholls A, Alexov E, Chiabrera A and Honig B. (2002) Rapid Grid-based Construction of the Molecular Surface for both Molecules and Geometric Objects: Applications to the Finite Difference Poisson-Boltzmann Method. J. Comp. Chem. 23, 128–137.

Santoro MM, Bolen DW. (1988) Unfolding free energy changes determined by the linear extrapolation method. 1. Unfolding of phenylmethanesulfo- nyl a-chymotrypsin using different denaturants. Biochemistry, 27: 8063–8068.

Schrödinger, LLC. (2010). The PyMOL Molecular Graphics System, Version 1.3r1.

Schumann FH, Riepl H, Maurer T, Gronwald W, Neidig K, Kalbitzer HR. (2007) Combined chemical shift changes and amino acid specific chemical shift mapping of protein-protein interactions. J Biomol NMR 39: 275–289.

Warren JR, Gordon JA (1966) On the Refractive Indices of Aqueous Solutions of Urea. J. Phys. Chem., 70: 297–300.